AERODYNAMICS OF SLENDER PRISMATIC BODIES

W.K. Tease and R.K. Cooper
Department of Aeronautical Engineering
Queen's University of Belfast
Belfast, U.K.

Abstract

A series of thick uncambered slender prismatic bodies, with diamond cross-sections, have been tested in a Low-Speed Wind Tunnel. Balance measurements, pressure plotting and flow visualisation tests were made to investigate the effects of thickness and aspect ratio on their aerodynamic characteristics.

The lift, drag and pitching moment coefficients increase smoothly up to about 30° angle of attack. The maximum L/D is about 4.3 for the bodies with thickness/span of 0.5, and the maximum lift coefficient is about 1. The lift efficiency with respect to both volume and planform area compares favourably to similar bodies of square or circular cross section.

Notation

C_L Lift coefficient, $Lift/(\frac{1}{2}\rho_\infty U_\infty^2 S)$

C_L' Volumetric Lift coefficient, $Lift/(\frac{1}{2}\rho_\infty U_\infty^2 Vol^{2/3})$

C_D Drag coefficient

C_z Normal force coefficient

C_x Axial force coefficient

C_{my} Pitching moment coefficient, moment reference at mid chord w.r.t each model.

C_p Pressure coefficient

S Planform area of model, (m²)

c Maximum chord length of model, (m)

α Angle of attack, (°)

AR Aspect ratio, $= b^2/S$

t Thickness of model, (m)

t/b Thickness to span ratio of model

s Semi-span, (m)

b Span, trailing edge, (m)

$X_{c.p.}$ Centre of pressure w.r.t apex of model, (m)

$$\frac{X_{c.p.}}{c} = \frac{X_o}{c} - \frac{M_y}{F_z c}$$

X_o Position of moment reference point w.r.t apex, (m)

Introduction

The technology of weapons is advancing into a new era. The shapes of missiles are radically changing, due to transfer of technology from stealth aircraft, F-117A, B2, ATF.[1,2,3] The concept of stealth is affecting the design of tactical subsonic stand-off missiles, of ground and sea skimming variants, in particular. Fig.1 shows a stand-off stealth missile concept proposed by Texas Instruments.[4,5]

Other changes are numerous and vary with the class of weapon; but generally a wider range of configurations, Mach number and increased manoeuvrability, are needed to keep pace with recent advances in fighter design and the need for missiles to intercept other missiles.[6,7]

In the design of modern day weapon configurations, it is necessary to know the characteristics of slender, low aspect ratio, monoplanar generic shapes.[8,9,10,17] We have investigated the subsonic aerodynamic characteristics of slender prismatic bodies whose shape is based on the facetted stealth design methodology. It is hoped the results presented in the paper will expand the database, enabling the applicability of semi-empirical methods to be extended, and will contribute to the validation of CFD methods.

Experimental Equipment and Procedure

Description of models

These generic shapes are a combination of a slender thick delta wing with or without a parallel after-body, each with a diamond cross-sectional shape. The model configurations are shown in Fig.5. Three thicknesses of model were tested; thickness to span ratio for model N1 = 0.33, N2 = 0.5, and N3 = 0.67. For each thickness the aspect ratio changed from 1, which coincides with the delta wing, to 0.2 by adding parallel after-bodies.

The thick delta wing noses were made from solid aluminium alloy, which was machined away internally to reduce weight. The afterbodies were of marine plywood construction. This robust afterbody ensured model deflections were kept to a minium. Mahogany laths were inlaid along the leading edges to ensure good edge definition. The models were sized to minimise wall interference effects and be capable of housing the strain gauge balance.

Support rig

The wings were supported in the wind-tunnel using a pitching swing arm sting mounted system. This rotated the model about its mid chord point keeping the model in the centre of the test section and minimising any flow interference effects. The sting itself represented an exhaust plume from an appropriate propulsion system. Sting extensions or

cranked attachments catered for the longer after bodies and higher angles of attack.

Two separate sting mounted strain gauge balances were used to obtain the normal force, pitching moment and the axial force. At large angles of incidence the sting bar and the strain-gauge balance deflected appreciably due to the aerodynamic loading. The angle of attack was corrected for sting deflection.

Experimental procedure

The test programme was carried put in a closed circuit wind tunnel with a working section of 1.143 m x 0.838 m, Fig.4. The test conditions were: Mach number 0.12; Reynolds number based on model span 0.54 million; and angle of attack range as follows.

Model No.	Alpha Range
Nn, NnB1	±45°
NnB2	±34°
NnB3, NnB4	±20°

Alpha was increased in 2° increments, unless a sudden change in a quantity required more detailed investigation.

Static surface pressure measurements were obtained for several chordwise stations, with and without boundary layer trips. The wing was assumed symmetrical so the wind-ward and lee-ward side pressures could be measured by simply inverting it.

A fluorescent oil flow technique was used to study the surface flow patterns on the models.

Wind tunnel corrections

The lift, drag and pitching moment coefficients were corrected for the effects of wind-tunnel solid and wake blockage. Kirkpatrick's blockage theory was used to estimate the total blockage. However as it is only valid for small alpha, Maskell's blockage correction was added to allow for the effect of the wake and separated flow regions at higher alpha[11,12,13]. No other corrections were made.

To illustrate the symmetry of the models and tunnel flow, the negative alpha quantities were mirrored onto the positive alpha values, eg. Figs. 13 & 14.

Results

The results are discussed in the light of previous work on the aerodynamics of thick slender wings.[11,14,15,18]

Non-linear lift generation
Thick slender delta wings

Lift coefficient for thick slender delta wings is plotted in Fig.6. As alpha increases from zero a non-linear relationship develops almost immediately, due to the flow separating from the sharp leading edges. Flow separation is apparent at about $\alpha = 2°$. Two conically shaped counterrotating vortices form on the leeward side of the model (Figs. 2, 23), and these cause low pressure regions near the leading edges. As alpha increases $dC_L/d\alpha$ increases, due to the strength of the vortices increasing. The boundary layer on the leeward side is accelerated under the primary vortex and then separates if the adverse pressure gradient is severe enough. The shear layer coils up and forms a secondary vortex, of opposite rotational sign, further outboard from the primary. Sometimes a tertiary separation occurs, producing another vortex, of opposite rotational sign yet again, situated slightly inboard of the secondary. The flow between the primary attachment lines p' is essentially streamwise.

Eventually $dC_L/d\alpha$ begins to decrease, and this is a sign of the wing being affected by vortex breakdown. The vortex burst has occurred down stream of the wing and moves upstream with increasing alpha. Once on the model it moves very quickly towards the apex region, refer to Figs. 27 & 28. As the thickness of the model increases α_{stall} is delayed to a higher value. It is not clear how thickness effects the propagation of the burst.

Slender prismatic bodies

The vortex flow structure develops with incidence over the leeward side of the fore-body of a slender prismatic body as described above for thick slender delta wings. When the vortex structure reaches the parallel after-body section it kinks so as to run approximately parallel to its edge in plan view, Fig.3. The primary reattachment lines p', secondary separation s and reattachment lines s' behave similarly with incidence but tertiary vortex flow from the fore-body is suppressed. This is due to the primary vortices lifting away from the surface at the junction, relieving the transverse adverse pressure gradient on the boundary layer and therefore it remains attached longer. This results in a shift of the secondary separation lines outboard. The distance above the surface of the primary vortices increases with axial distance, thus reducing their influence. The surface streak pattern gradually becomes more streamwise. The secondary separation lines diverge gradually, the extent depending upon the length of the after-body, refer to Figs. 24, 25.

Thickness effect on lift

In agreement with previous work, reduction in overall lift occurs as wing thickness is increased, Fig.6.[11,15,18] The linear component of the lift falls as well as the non-linear component. This is true for the slender prismatic bodies as well as delta wings.

Effect of aspect ratio on lift

Slender prismatic bodies

The non-linear variation of C_L with α is shown in Fig.11. At a given α the larger the AR the greater the lift. Thus the vortex structure over a delta wing is more efficient at producing lift than the structure over a prismatic body. This is due to the reduced amount of vorticity being shed into the flow from the after-body and the movement of the primary vortices away from the surface, thus reducing their influence.

Tests on N2B3 and N2B4 were stopped at $\alpha = 20°$ due to test section size restrictions. As α increases further N2B2 shows symptoms of beginning to stall; $dC_L/d\alpha$ decreases. The test was stopped at $\alpha = 34°$ again due to test section size restrictions. For $\alpha > 28°$ N2B1 performs better than N2, and stall data is as follows.

Model No.	α_{stall}	C_{Lmax}
N2	36°	1.04
N2B1	36°	1.07
N2B2	>36°	>1.0

Thickness effect on drag

At zero angle of attack drag is composed of base pressure drag plus skin friction drag. With these bodies being bluff shaped the base pressure is the primary drag component and hence the model with the largest base area/ wing area will have the largest drag coefficient. This is illustrated in Figs.7 and 12 for the delta wings and prismatic wings respectively.

As alpha increases the drag varies non-linearly. Induced drag is caused by the vortex system on the leeward side of the wing, and this adds onto the zero lift dependent drag. The induced drag increases with the increasing circulation of the vortex system. The strength of the vortex is controlled primarily by increasing alpha or secondly decreasing thickness. Another secondary effect based on thickness occurs concurrently with the above. With increasing wing thickness, the suction forces induced by the leading edge vortices have an increasingly forward component

in the plane of the wing (ie. leading edge thrust) and consequently, the lift dependent drag of a thick wing is less than that of a thin wing, with the same planform. Refer to Fig.22 to see the effect leading edge thrust has in overcoming the axial force due to skin friction plus the base pressure. The kink in the C_X curves is due to the vortex burst moving over the wings.

Effect of aspect ratio on drag

Fig.16 shows C_D vs C_L for the slender prismatic bodies. At zero angle of attack the drag coefficient decreases with decreasing AR, due to the decreased base area/ wing area, as discussed above. If the zero lift drag is subtracted, the curves are remarkably similar. The lift dependent drag is approximately proportional to C_L^2 up to $C_L = 1$.

Results for C_L/C_D

As the thickness of the model decreases $(C_L/C_D)_{max}$ increases and occurs at a lower α, as shown in Fig.8 and the table below.

Model No.	α	$(C_L/C_D)_{max}$
N1	10.7°	3.2
N2	13.8°	2.4
N3	16.9°	1.9

This is also true for the slender prismatic bodies, although the results are not presented here. For the slender prismatic bodies, as the AR decreases, then $(C_L/C_D)_{max}$ increases and occurs at a lower α, as shown in Fig.13 and the table below.

Model No.	α	$(C_L/C_D)_{max}$
N2	13.8°	2.4
N2B1	9.6°	3.6
N2B2	8°	4.3
N2B3	8°	4.3
N2B4	8°	4.3

Lift and volume

Lift coefficient based on volume to the power 2/3 vs alpha is given in Fig.17. This shows that the prismatic bodies have a similar lifting volumetric efficiency for $\alpha > 10°$, and the maximum value exceeds that for the delta wing. For lower alpha the

lift curve slope is higher for the higher aspect ratio wings. The volumetric lift coefficient compares favourably to that for a square cross section body of length/ span ratio 9.[8] For a slender prismatic body of square cross section, the volumetric lift coefficient at $\alpha = 20°$ is about 0.88, compared with 1.9 for N2B4. The corresponding value for an axisymmetric body is about 0.29[8]. The high lift efficiency with respect to both volume and planform area is a notable feature of these slender prismatic bodies. This implies that highly manoeuvrable vehicles may be designed.

Longitudinal Static Stability

It is assumed, with respect to longitudinal static stability considerations, that the centre of gravity is positioned at the mid chord point (on the centre-line), thus the pitching moment is taken about this point for each model. (Positive C_{my} is a nose up pitching moment, in the same sense as alpha).

Referring to Figs. 9 & 10 it can be seen that the delta wings are stable up to $\alpha = 30°$ approximately. C_{my} varies non-linearly with alpha, $dC_{my}/d\alpha$ increasing gradually from 0° to 30°, due to the ordered vortex flow structure. For alpha greater than approximately 30° C_{my} becomes highly non-linear due to vortex interactions and vortex burst occurring over the model, as confirmed by the flow visualization, Figs. 26, 27 & 28. As the models become thicker they become marginally more stable. Increasing thickness also delays vortex burst propagation. This is highlighted by N3, Fig.9 where C_{my} does not go severely non-linear until $\alpha = 35°$.

For the slender prismatic bodies, C_{my} behaves non-linearly with alpha (Fig.14) for the same reasons as described for the thick delta wings. As the aspect ratio decreases the stabilising pitching moment reduces until it becomes destabilising for AR < 0.33. The destabilising effect of vortex burst is visible for $\alpha > 30°$. Fig.15 shows the progressive forward shift of centre of pressure, $X_{c.p}/c$, as the afterbody length increases. This illustrates that the delta wing forebody generates more lift per unit area than the parallel afterbody. Lifting surfaces may be added to the rear of the longer bodies to move the centre of pressure aft, and produce a stable pitching moment curve.

Static pressure distribution

Figs. 18 and 19 show typical pressure coefficient distributions on N2 at 72.3% chordwise station, without boundary layer tripping. Note the change in suction peak type as the angle of attack increases above 20°, due to the boundary layer transition from laminar to turbulent. The positions of the suction peaks move as alpha increases, and this coincides with the movement of separation and reattachment lines of the various flow structures already described.

Some flow asymmetry is visible both on the windward and leeward sides. This could be due to several factors: (a) wind-tunnel flow asymmetry, (b) model asymmetry (althought this is small), (c) model set at slight yaw or roll angle. Note the falling off of the leeward side (negative) pressure coefficient distribution for $\alpha > 30°$ and the asymmetry. Due to asymmetric vortex burst, the left hand suction peak is smeared out, reducing the adverse pressure gradient and allowing the secondary separation lines to move out spanwise (Figs. 27,28). The burst vortex influence spreads slightly over onto the other half of the model, due to the slenderness of the body. The other vortex structures remain intact. The asymmetric vortex burst will cause a rolling moment, but this has not been evaluated.

Boundary layer tripping

Figs. 20 and 21 illustrate the effect of boundary layer trips on the normal force and spanwise static pressure distribution. The spanwise pressure distribution changes from laminar to turbulent profile type, but there is little effect on forces and moments. There is virtually no change in normal force coefficient C_z up to $\alpha = 37°$.

Conclusions

All the slender prismatic bodies display favourable aerodynamic characteristics over the range of angle of attack tested, in particular, the smooth non-linear variations of C_L, C_D and C_{my} as α increases, up to 30°. Vortex burst propagation causes an unstable break in C_{my} for larger α, with asymmetric pressure distributions. This is delayed to about $\alpha = 35°$ for the thickest delta wing. It appears that rolling moment and yawing moment may be very sensitive to such flow asymmetry. Generally for prismatic bodies the greater the AR the greater the lift generated. An exception to this is illustrated when N2B1 out performs N2 at high alpha.

The lift efficiency based on planform area or volume$^{2/3}$ compares favourably with similar slender bodies of square or circular cross section. The maximum L/D is about 4.3 for the prismatic bodies with thickness/span of 0.5.

Due to the slender, parallel afterbodies, a useful geometric property of the diamond cross-section is its volumetric efficiency, when the bodies are packed in close proximity to one another. Stealth aircraft have had to carry their weapons concealed inside the airframe, to prevent an increase in the aircraft's Radar Cross-section Signature (RCS). These shapes because of their own low RCS will be able to blend, (bodily conform) into the shape of the airframe, thus saving valuable space.

References

1   Richardson, D.: Stealth Warplanes. Pub. Guild, 1989.

2   Sweetman, B.: Stealth Bomber, Pub. Airlife, 1989

3   Fuhs, A.E.: Radar Cross Section Lectures, US Naval Postgraduate School, Monterey California, Publ. American Institute of Aero and Astronautics, 1633 Broadway,NY 10019

4   Texas Instruments Reveals its Design for New Navy Stand-off Weapon, Aviation Week & Space Technology, Oct. 30, 1989

5   Lenorovitz, J.M.: Italians Redesigning Skyshark to Improve Stealth Qualities, Aviation Week & Space Technology, Feb. 17, 1992

6   Foster, D.N.: Weapon Aerodynamics, Aerospace, June 1989, pp8-14; also RAE TM Aero 2150, 1989.

7   Fulghum, D.A.: Industry Designing Stealthy Sidewinder for Next-Generation Navy/USAF Aircraft,Aviation Week & Space Technology, May 20, 1991

8   Brebner, G.G.; Osborne, W.K. & Brown, D.E.: Force and Moment Wind Tunnel Measurements at Mach Numbers from 0.6 to 2.0 on a Body of Square Cross-Section, Alone and in Conbination with Cruciform Delta Wings of Aspect Ratio 0.52, RAE TR 81034, 1981

9   Brebner, G.G.; Osborne, W.K. & Brown, D.E.: Force and Moment Wind Tunnel Measurements at Mach Numbers from 0.6 to 2.8 on Two Flat-Topped Bodies, Alone and in Combination with a High Delta Monoplane Wing of Aspect Ratio 0.83, RAE TR 81035, 1981

10   Howarth, R.N.L.: Investigation of the Aerodynamic Characteristics of a Square-Bodied Lifting Dispenser in the 8ft x 6ft Transonic Wind Tunnel, RAE TM Aero 2108, 1987.

11   Kirkpatrick, D.L.I.: Investigation of the Normal Force Characteristics of Slender Delta Wings With Various Rhombic Cross-sections in Subsonic Conical Flow. ARC CP 922, RAE TR 65291, 1965.

12   Maskell, E.C.: A Theory of the Blockage Effects on Bluff Bodies and Stalled Wings in a Closed Wind-Tunnel, RAE R & M 3400, 1963

13   Gilli, P.A.; Pastrone, D.M. & Quagliotti, F.B.: Blockage Corrections at High Angles of Attack in a Wind-Tunnel, ICAS-88-3.8.3, 1988

14   Kirby, D.A. & Kirkpatrick, D.L.I.: An Experimental Investigation of the Effect of Thickness on the Subsonic   Longitudinal Stability Characteristics of Delta Wings of 70 degs Sweep-back. RAE TR 69256, 1969.

15   Smith, J.H.B. & Kurn, A.G.: Pressure Measurements on Slender Rhombic Cones at Incidence at Mach Numbers 0.4 to 1.1. RAE TR 68171, 1968; ARC R&M 3626, 1970.

16   Stallings, R.L.: Low Aspect Ratio Wings at High Angle of Attack, in Tactical Missile Aerodynamics, ed. Hemsch, M.J. & Nielsen, J.N., *Progress in Astronautics and Aeronautics*, Vol.104, AIAA, 1986, pp89-128.

17   Jackson, C.M. and Sawyer, W.C.: Bodies with Non-circular Cross Sections and Bank-to-Turn Missiles, *ibid*. pp168-197.

18   Russell, S.C.: The Effects of Conical Thickness on the Flow About Low Aspect Ratio Wings with Sharp Leading Edges, PhD. thesis, University of Salford, Mechanical Engineering Dept., 1969.
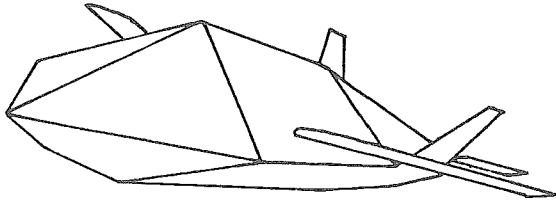
Fig.1. Texas Instruments Stealth missile concept
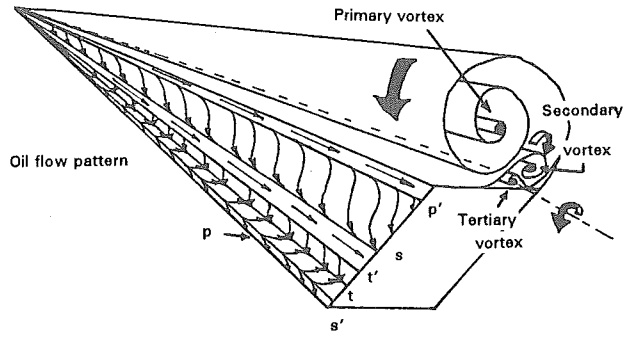
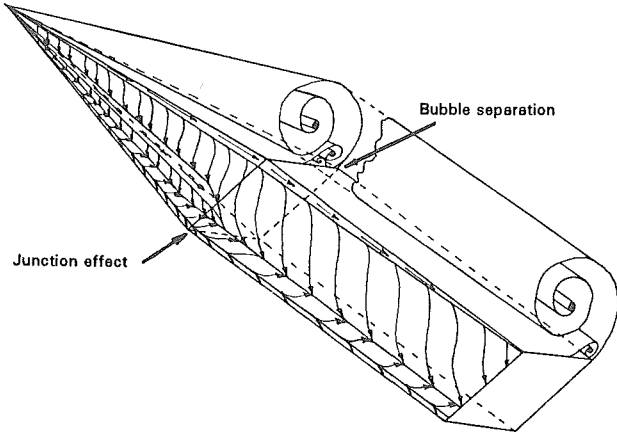Fig.2. Vortex flow structure over a thick delta wing

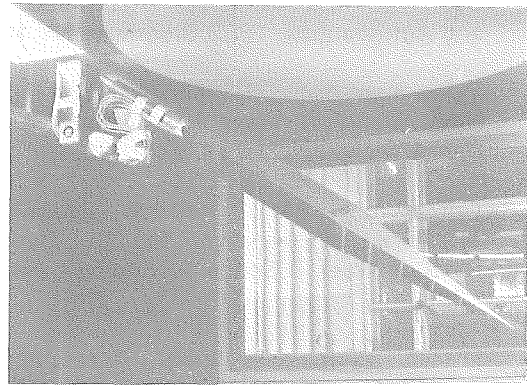Fig.3. Vortex flow structure over a slender prismatic body
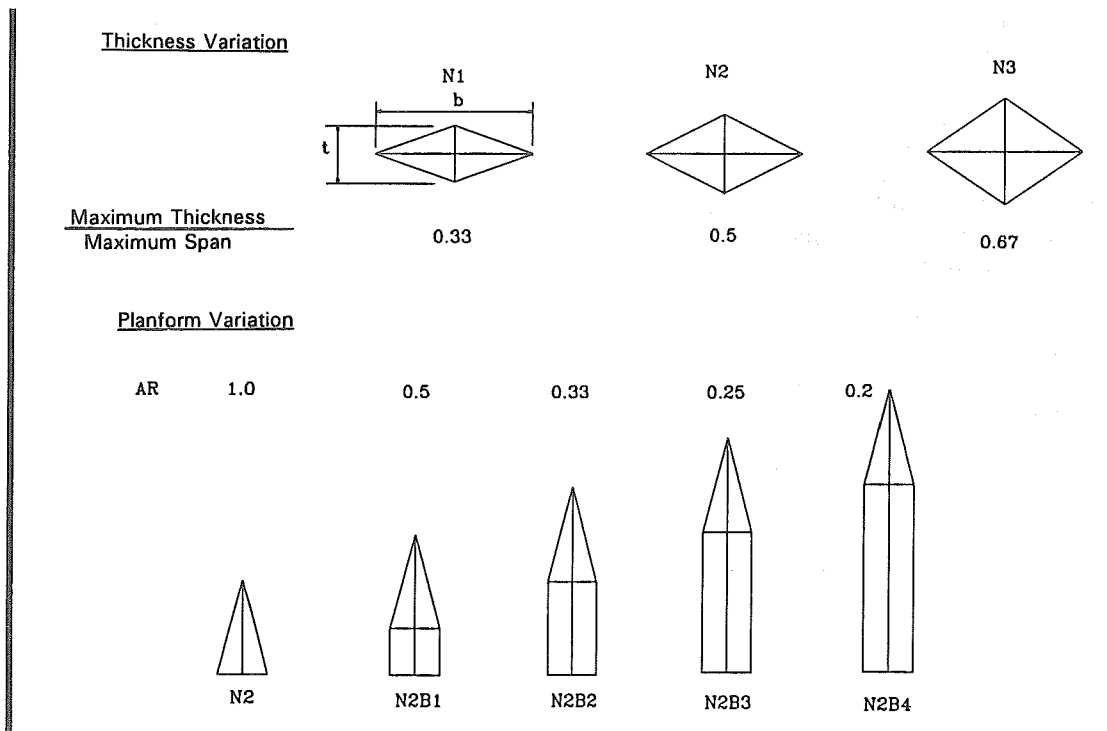

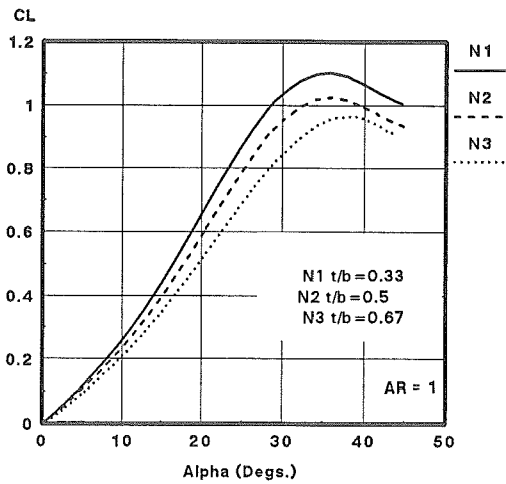Fig.4. Wind-tunnel test-section setup

Fig.5. Model test configurations
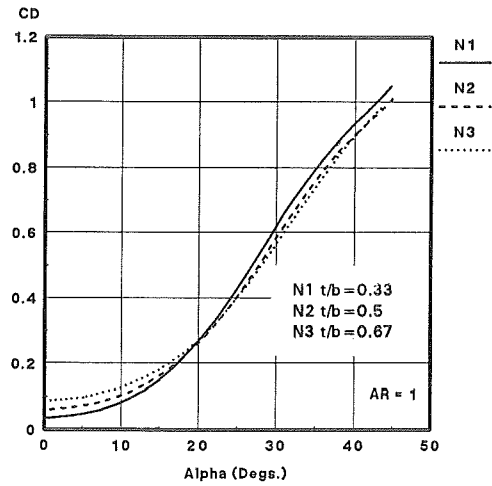
CL

1.2

1

0.8

0.6

0.4

0.2

0

N1
N2
N3

N1 t/b=0.33
N2 t/b=0.5
N3 t/b=0.67

AR = 1

0   10   20   30   40   50
Alpha (Degs.)

Fig.6. C_L vs α for slender delta wings

with thickness, untripped test

CD

1.2

1

0.8

0.6

0.4

0.2

0

N1
N2
N3

N1 t/b=0.33
N2 t/b=0.5
N3 t/b=0.67

AR = 1

0   10   20   30   40   50
Alpha (Degs.)

Fig.7. C_D vs α for slender delta wings

with thickness, untripped test

CL/CD

3.5

3

2.5

2

1.5

1

0.5

0

N1

N2

N3

N1 t/b=0.33
N2 t/b=0.5
N3 t/b=0.67

AR = 1

0   10   20   30   40   50
Alpha (Degs.)

Fig.8. C_L/C_D vs α for slender delta wings

with thickness, untripped test

Cmy

0

-0.02

-0.04

-0.06

-0.08

-0.1

-0.12

-0.14

N1

N2

N3

N1 t/b=0.33
N2 t/b=0.5
N3 t/b=0.67

AR = 1

0   10   20   30   40   50
Alpha (Degs.)

Fig.9. C_{my} vs α for slender delta wings

with thickness, untripped test

X c.p./c

0.75

0.7

0.65

0.6

0.55

0.5

0.45

N1

N2

N3

0   10   20   30   40   50
Alpha (Degs.)

N1 t/b=0.33
N2 t/b=0.5
N3 t/b=0.67   AR = 1

Fig.10. $X_{c.p.}/c$ vs α for slender delta wings

with thickness, untripped test.

CL

1.2

1

0.8

0.6

0.4

0.2

0

N2

N2B1

N2B2

N2B3

N2B4

0   10   20   30   40   50
Alpha (Degs.)

N2 AR=1
N2B1 AR=0.5
N2B2 AR=0.33

N2B3 AR=0.25
N2B4 AR=0.2

Fig.11. C_L vs α for slender prismatic bodies

with varying AR, untripped test

2050
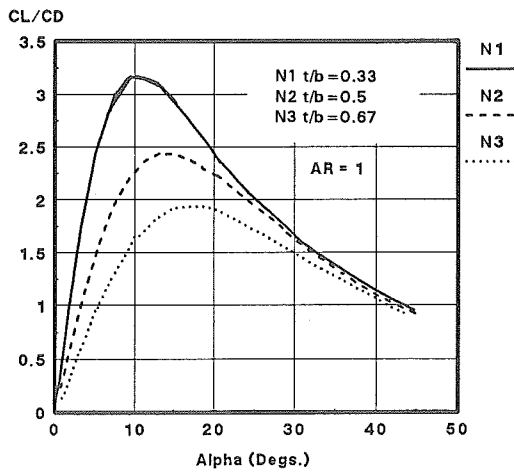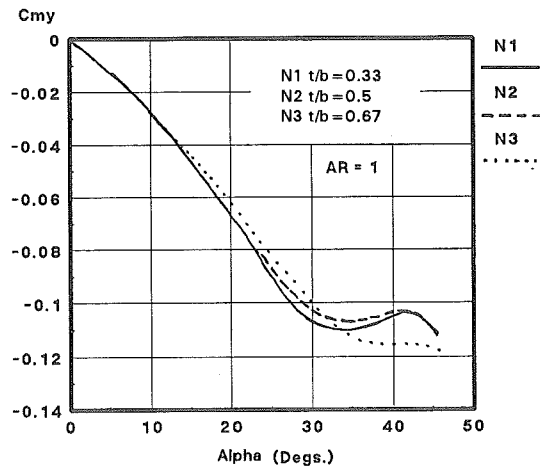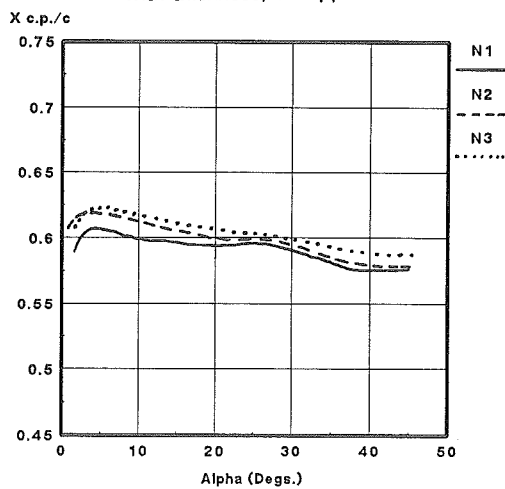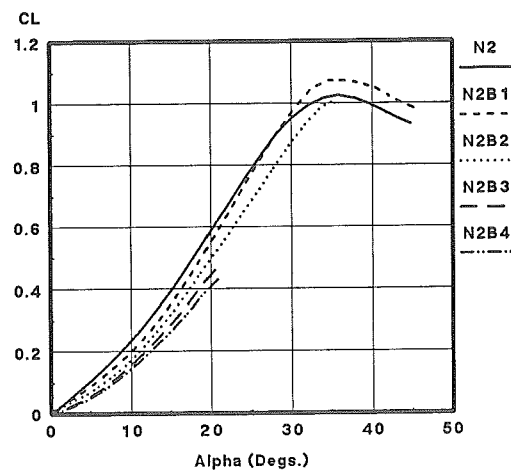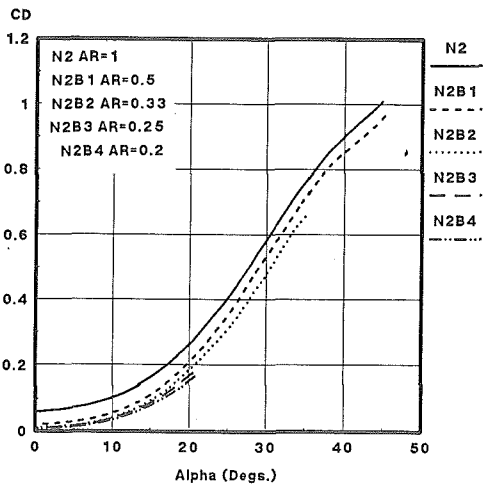
Fig.12. C_D vs α for slender prismatic bodies with varying AR, untripped test
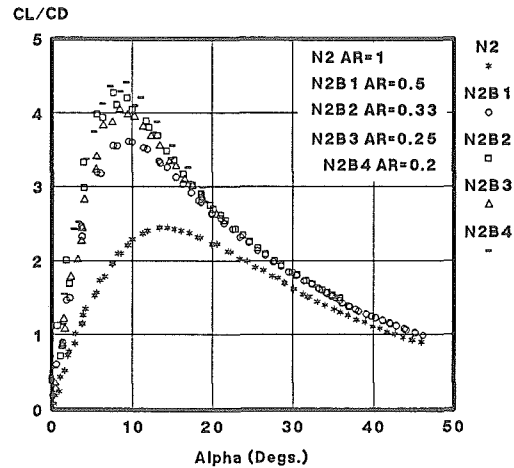
Fig.13. C_L/C_D vs α for slender prismatic bodies with varying AR, untripped test
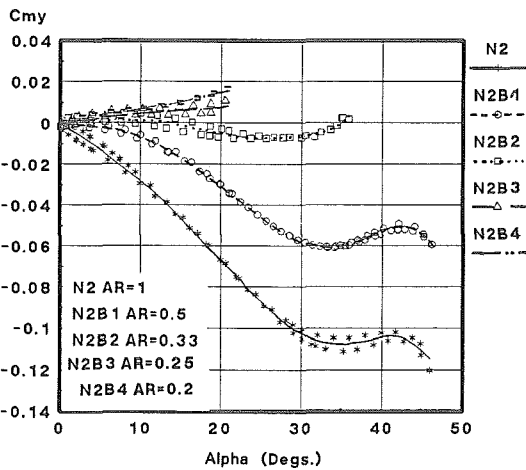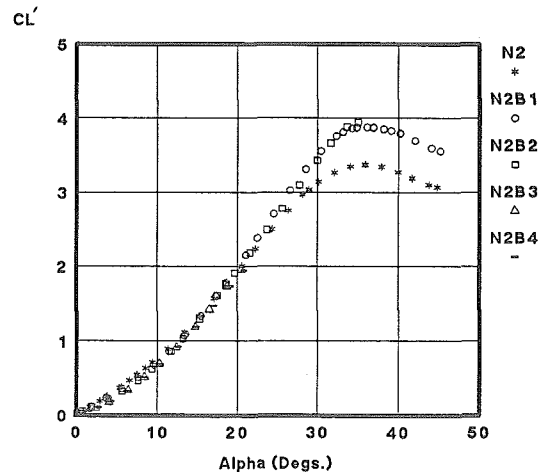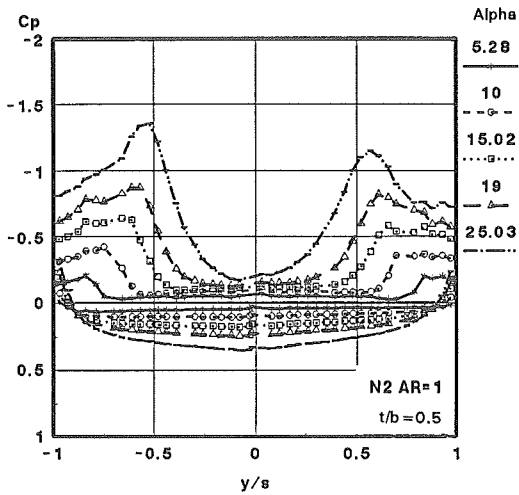
Fig.14. C_{my} vs α for slender prismatic bodies with varying AR, untripped test
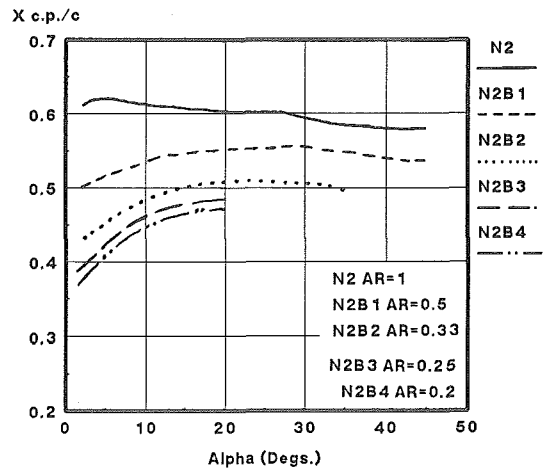
Fig.15. $X_{c.p.}/c$ vs α for slender prismatic bodies with varying AR, untripped test.
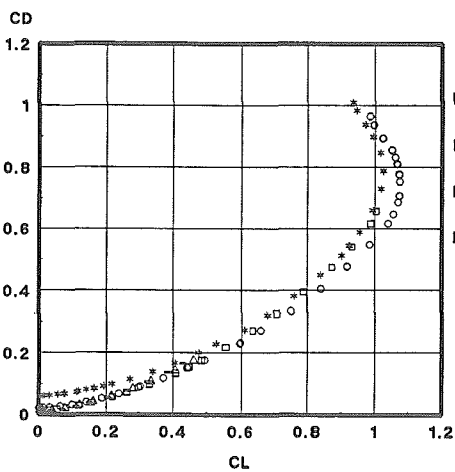
Fig.16. C_D vs C_L for slender prismatic bodies with varying AR, untripped test

Fig.17. C_L' vs α for slender prismatic bodies with varying AR, untripped test

N2 AR=1
N2B1 AR=0.5
N2B2 AR=0.33
N2B3 AR=0.25
N2B4 AR=0.2

N2 AR=1
N2B1 AR=0.5
N2B2 AR=0.33
N2B3 AR=0.25
N2B4 AR=0.2

Fig.18. Spanwise static pressure distribution on N2 at 72.3% chordwise station, untripped test
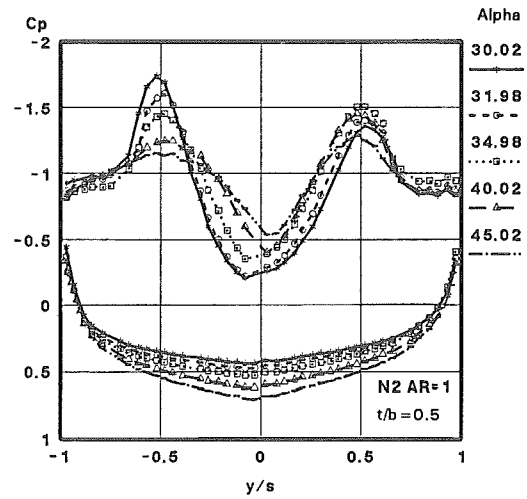
Fig.19. Spanwise static pressure distribution on N2 at 72.3% chordwise station, untripped test
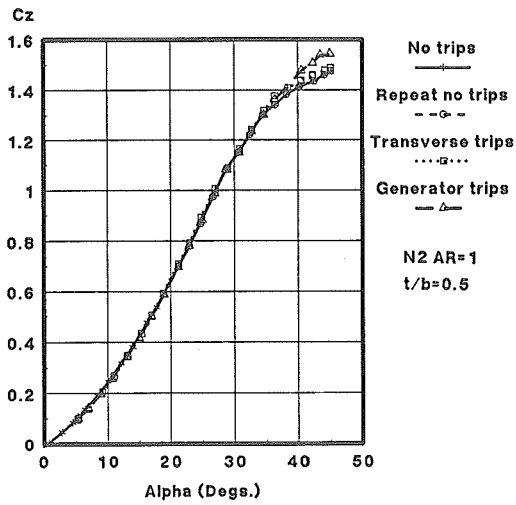
Fig.20. Effect of boundary layer tripping on force results
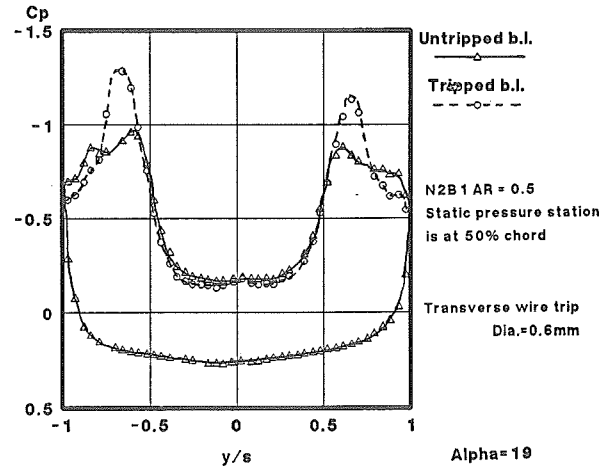
Fig.21. Change in spanwise static pressure distribution due to boundary layer trips
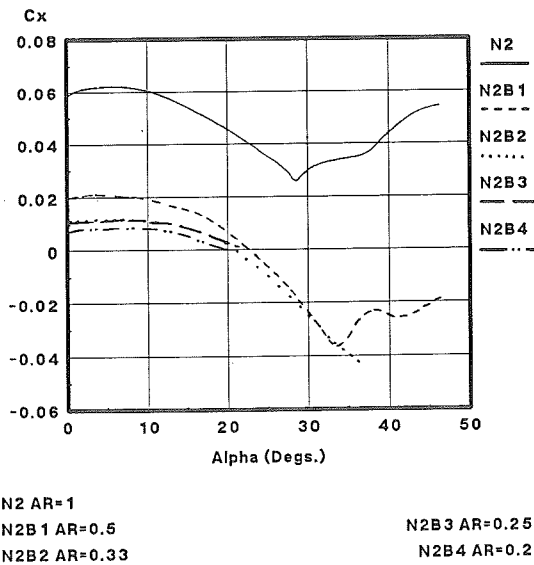
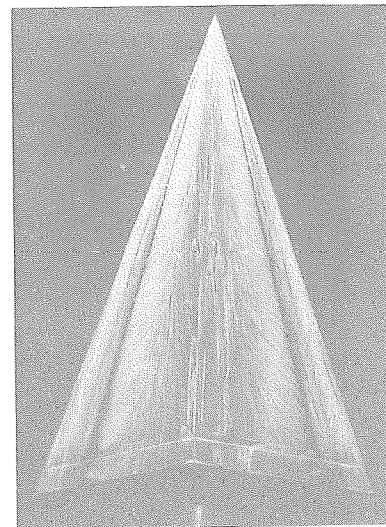Fig.22. Leading edge thrust effect on C_x vs α with varying AR
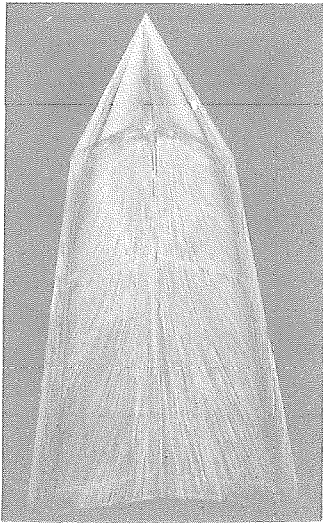

Fig.23. N2 oil flow pattern, $\alpha = 15°$

Fig.24. N2B2 oil flow pattern, $\alpha = 15°$
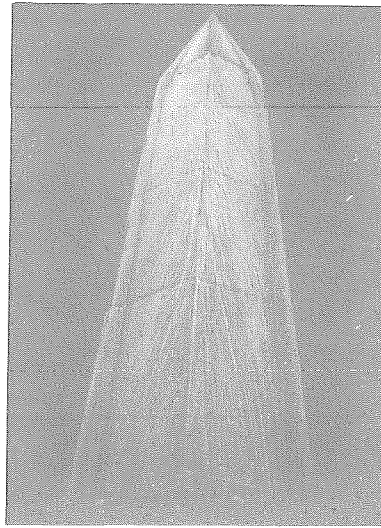
Fig.25. N2B4 oil flow pattern, $\alpha = 15°$
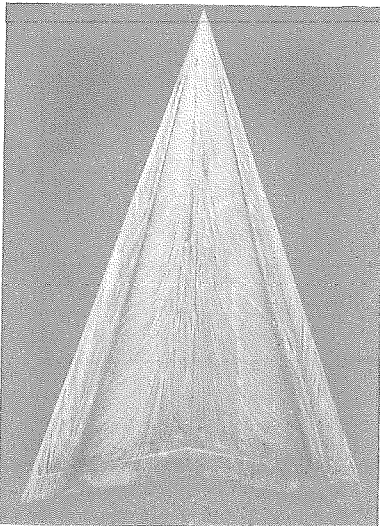
Fig.26. N2 oil flow pattern, $\alpha = 19°$

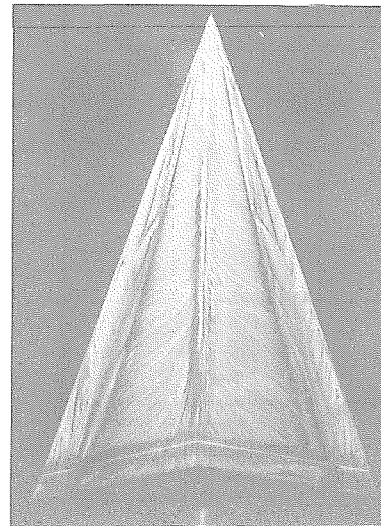Fig.27. N2 oil flow pattern, $\alpha = 30°$
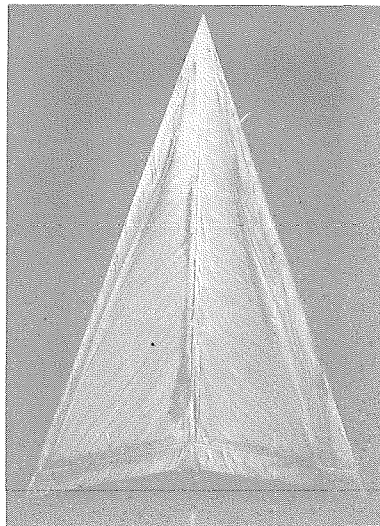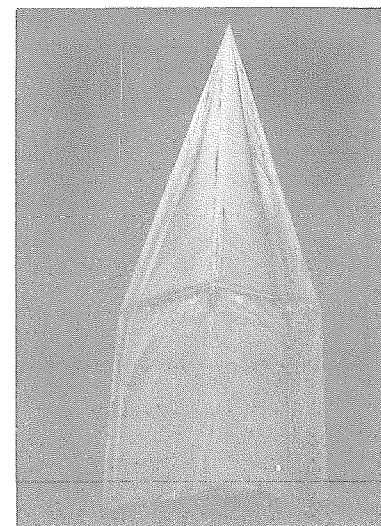

Fig.28. N2 oil flow pattern, $\alpha = 40°$

Fig.29. N2B1 oil flow pattern, $\alpha = 40°$